

# UC Davis

## UC Davis Previously Published Works

### Title

N-dihydrogalactochitosan reduces mortality in a lethal mouse model of SARS-CoV-2.

### Permalink

<https://escholarship.org/uc/item/5dg380kj>

### Journal

PLoS One, 18(8)

### Authors

Weiss, Christopher  
Liu, Hongwei  
Ball, Erin  
et al.

### Publication Date

2023

### DOI

10.1371/journal.pone.0289139

Peer reviewed

## RESEARCH ARTICLE

## N-dihydrogalactochitosan reduces mortality in a lethal mouse model of SARS-CoV-2

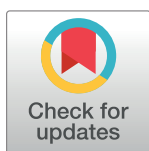
Christopher M. Weiss<sup>1#a</sup>, Hongwei Liu<sup>1</sup>, Erin E. Ball<sup>1#b</sup>, Ashley R. Hoover<sup>2</sup>, Talia S. Wong<sup>1</sup>, Chun Fung Wong<sup>3</sup>, Samuel Lam<sup>3</sup>, Tomas Hode<sup>3</sup>, M. Kevin Keel<sup>1</sup>, Richard M. Levenson<sup>4</sup>, Wei R. Chen<sup>2</sup>, Lark L. Coffey<sup>1\*</sup>

**1** Department of Pathology, Microbiology & Immunology, University of California, Davis, California, United States of America, **2** Stephenson School of Biomedical Engineering, University of Oklahoma, Norman, Oklahoma, United States of America, **3** Immunophotonics, Inc., Saint Louis, Missouri, United States of America, **4** Department of Pathology and Laboratory Medicine, UC Davis Health, Sacramento, California, United States of America

#a Current address: MRIGlobal, Kansas City, Missouri, United States of America

#b Current address: Armed Forces Research Institute of Medical Sciences (AFRIMS), Bangkok, Thailand

\* [lcoffey@ucdavis.edu](mailto:lcoffey@ucdavis.edu)



## OPEN ACCESS

**Citation:** Weiss CM, Liu H, Ball EE, Hoover AR, Wong TS, Wong CF, et al. (2023) N-dihydrogalactochitosan reduces mortality in a lethal mouse model of SARS-CoV-2. *PLoS ONE* 18(8): e0289139. <https://doi.org/10.1371/journal.pone.0289139>

**Editor:** Engin Berber, Lerner Research Institute - Cleveland Clinic, UNITED STATES

**Received:** March 8, 2023

**Accepted:** July 11, 2023

**Published:** August 8, 2023

**Copyright:** This is an open access article, free of all copyright, and may be freely reproduced, distributed, transmitted, modified, built upon, or otherwise used by anyone for any lawful purpose. The work is made available under the [Creative Commons CC0](https://creativecommons.org/licenses/by/4.0/) public domain dedication.

**Data Availability Statement:** Data are available at Zenodo via this link: [10.5281/zenodo.7709464](https://doi.org/10.5281/zenodo.7709464).

**Funding:** Funding support was provided by the UC Berkeley Henry Wheeler Center for Emerging and Neglected Diseases (CEND) COVID Catalyst Fund, and internal funding from the UC Davis Office of the Vice Chancellor of Research. The funders had no role in study design, data collection and analysis, decision to publish, or preparation of the manuscript.

## Abstract

The rapid emergence and global dissemination of SARS-CoV-2 that causes COVID-19 continues to cause an unprecedented global health burden resulting in nearly 7 million deaths. While multiple vaccine countermeasures have been approved for emergency use, additional treatments are still needed due to sluggish vaccine rollout, vaccine hesitancy, and inefficient vaccine-mediated protection. Immunoadjuvant compounds delivered intranasally can guide non-specific innate immune responses during the critical early stages of viral replication, reducing morbidity and mortality. N-dihydrogalactochitosan (GC) is a novel mucoadhesive immunostimulatory polymer of  $\beta$ -0-4-linked N-acetylglucosamine that is solubilized by the conjugation of galactose glycans with current applications as a cancer immunotherapeutic. We tested GC as a potential countermeasure for COVID-19. GC was well-tolerated and did not produce histopathologic lesions in the mouse lung. GC administered intranasally before and after SARS-CoV-2 exposure diminished morbidity and mortality in humanized ACE2 receptor expressing mice by up to 75% and reduced infectious virus levels in the upper airway. Fluorescent labeling of GC shows that it is confined to the lumen or superficial mucosa of the nasal cavity, without involvement of adjacent or deeper tissues. Our findings demonstrate a new application for soluble immunoadjuvants such as GC for preventing disease associated with SARS-CoV-2 and may be particularly attractive to persons who are needle-averse.

## Importance

The ongoing COVID-19 pandemic necessitates new approaches to reduce disease caused by SARS-CoV-2. We tested the immunoadjuvant N-dihydrogalactochitosan (GC), used previously as an immunostimulant for tumor therapy and adjuvant for viral vaccines, as a potential COVID-19 countermeasure. When GC was administered before and after inoculation of a

**Competing interests:** TH, CFW, SSKL declare a conflict of interest as employees with minority ownership stakes of Immunophotonics, Inc., the manufacturer of the proprietary immune stimulant GC. RML declares a conflict of interest as an advisor with minority ownership stake in Immunophotonics. This does not alter our adherence to PLOS ONE policies on sharing data and materials.

lethal dose of SARS-CoV-2 into the nose of humanized mice expressing an entry receptor for the virus, fewer mice showed weight loss and died compared to mice that received only the vehicle but no GC. GC-treated mice also had lower levels of infectious SARS-CoV-2 in their upper airway. These results suggest that GC may be a candidate to prevent or treat COVID-19.

## Introduction

Severe acute respiratory syndrome-like coronavirus 2 (SARS-CoV-2) that was first identified from a cluster of viral pneumonia cases in Wuhan, China in December 2019 [1] has caused more than 670 million cases and nearly 6.9 million deaths globally as of March 2023 [2]. Clinical manifestations of 2019 novel coronavirus disease (COVID-19) caused by SARS-CoV-2 typically include fever, non-productive cough, and mild to moderate dyspnea, with severe cases developing pneumonia and acute respiratory distress syndrome [1,3,4]. SARS-CoV-2 morbidity and mortality increase with age and systemic proinflammatory and cardiovascular co-morbidities [1,3,5]. Recovered patients may also exhibit long-duration symptoms including disruption to sensations of taste and smell, and cognitive impairment (colloquially referred to as “brain fog”) resulting from neurological involvement [6,7].

Like SARS-CoV, SARS-CoV-2 uses the angiotensin converting enzyme 2 (ACE2) for cell entry [8,9]. Small animals including mice, hamsters, and ferrets, have been fundamental in defining SARS-CoV-2 pathogenesis and developing medical countermeasures [10,11]. Transgenic mice expressing the human ACE2 (hACE2) gene from the human cytokeratin 18 (K18) promoter have served as an especially useful model of severe disease due to well characterized genetics and ease of use [12–14]. Intranasal inoculation of K18-hACE2 mice (hereafter termed hACE2) with SARS-CoV-2 results in a high viral burden in the lungs, which diminishes past day 7, and elevated viral loads detectable in the brain at day 7 [13].

SARS-CoV-2, which can be transmitted in small-droplet aerosols from person to person, can take up to 14 days to produce symptoms [15]. Public health countermeasures have evolved as additional treatments and information regarding transmission risks for COVID-19 have become available. In addition to face coverings and physical distancing, multiple vaccine candidates and therapeutic interventions have now received authorization by the United States Food and Drug Administration (FDA) [16]. While ‘herd immunity’ through vaccination remains the target, it is estimated that 70–90% of the global population must be immune in order to interrupt transmission [17]. This target becomes even more challenging with high levels of vaccine skepticism, slow production, inequitable distribution, and the rise of variants of concern capable of more efficient transmission or vaccine escape. Pre- and post-exposure countermeasures can help fill the vaccine gap by reducing COVID-19 morbidity and mortality in unprotected communities and thus reduce the global burden of the pandemic. The nucleoside analog, remdesivir [18] and the protease inhibitor paxlovid [19] are the only current FDA-approved therapeutics approved for non-hospitalized COVID-19 patients and were authorized based on their ability to shorten recovery time [20], but are not ideal for clinical use due to their moderate clinical efficacy [21], and remdesivir requires intravenous administration. Although there are many active trials of therapeutic agents with more than 10 drugs or biological products holding emergency use authorization, most are indicated for patients with severe COVID-19 [22,23]. Despite these advances, there are presently no drugs available for high-risk exposure use to protect against SARS-CoV-2. To circumvent this gap, we repurposed an immunostimulant used for cancer immunotherapy and as a vaccine adjuvant with a goal of mitigating COVID-19 disease.

The parent compound of GC, chitosan, is a linear biological polysaccharide polymer of  $\beta$ -D-4-linked N-acetylglucosamine and is produced from alkaline treatment of the chitin

exoskeleton of crustaceans. Chitosan is approved by the FDA for tissue engineering and drug delivery. Chitosan shows broad-acting antiviral [24] and immunoadjuvant properties [25,26] including interferon (IFN) induction [27,28] that is critical for viral control [29–31], has been evaluated as an antiviral therapy for respiratory viruses [32–34] and shows antiviral activity against the porcine coronavirus pathogen porcine epidemic diarrhea virus [35]. Chitosan and various derivatives have been explored as COVID-19 treatments and vaccine adjuvants [36–41]. Modification of chitosan by covalently attaching galactose sugars to the free amino acids on the polysaccharide backbone produces N-dihydrogalactochitosan (GC) [42,43]. GC was initially designed to further improve immune-stimulating functionality of the molecular backbone by adding glycan moieties that can bind to C-type lectin receptors on antigen presenting cells [44] and lead to a downstream immune response while retaining the mucoadhesive properties of the parent molecule [45]. Furthermore, GC has improved solubility at physiological pH ranges compared to its parent molecule, and hence is more suitable as an injectable agent. With these modifications, GC has been developed for use in human interventional immuno-oncology to stimulate systemic anti-tumor immunity [46]. GC recruits granulocytes at the injection site [47] and stimulates activation of dendritic cells and macrophages through upregulation of co-stimulatory molecules CD40, CD86, and MHCII *in vitro* and *in vivo* [48,49]. Macrophages also show increased nitric oxide production and phagocytic abilities in response to GC [48]. Single-cell RNA sequencing indicates enrichment of type I IFN signaling in multiple innate immune cells, including monocytes, M1 macrophages, and neutrophils in tumors following GC administration [50]. Our prior work showed that GC mixed with recombinant SARS-CoV-2 spike and nucleocapsid antigen vaccines delivered intranasally protects mice from lethal disease after intranasal SARS-CoV-2 inoculation. In that study, when 0.75% GC was delivered intranasally to control mice, CD45<sup>+</sup> and B cell cellularity increased in cervical lymph nodes accompanied by an influx of migrating and resident dendritic cells and CD4<sup>+</sup> and CD8<sup>+</sup> T cells. These data show that GC induces a local immune response that induces lymphocyte migration and activation in the nasal-associated lymphoid tissue (NALT) [51]. The upregulation of innate immune responses and recruitment of cellular responses to the NALT, which is the SARS-CoV-2 exposure site, suggests that broad-acting non-toxic immunoadjuvants such as GC that can be intranasally may modulate SARS-CoV-2 infection. Intranasal instillation may generate a robust immune protection in the upper respiratory tract and may be more widely accepted than vaccine injections. Furthermore, non-specific immunoadjuvants such as GC could offer a benefit over more narrowly targeted antivirals by providing protection against a broad range of pathogens, potentially including future agents not yet affecting public health.

In the present study, we explored the use of GC for prophylaxis against SARS-CoV-2 infection applied pre- and post-exposure to lethal dosages of the virus in transgenic hACE2 mice. To simulate the use of solubilized GC as a nasal spray, we applied the compound intranasally twice before exposure and once following exposure of mice to a human isolate of SARS-CoV-2. Our data demonstrate a strong protective effect of GC in preventing mortality in this lethal model of disease. Fluorescent-labeled GC administered intranasally remained in the nasal cavity. Pre- and post-exposure countermeasures may help fill the vaccine gap by reducing COVID-19 morbidity and mortality and reduce the continued global burden of the pandemic.

## Results

### N-dihydrogalactochitosan reduces SARS-CoV-2-associated mortality in hACE2 transgenic mice

To determine the antiviral efficacy of N-dihydrogalactochitosan (GC) against SARS-CoV-2, 6-week-old hACE2 [B6.Cg-Tg(K18-ACE2)2Prlmn/J] mice were treated intranasally (i.n.) with

0.75% GC in neutral buffered saline 3 and 1 days prior to virus exposure and then 1 day post exposure (Fig 1a). This dose was selected since our prior dose response studies showed that GC stimulates migration and activation of lymphocytes in the NALT [51]. To ensure that the dose, schedule, and route of GC administration were well tolerated, pilot studies using 14 additional male and female hACE2 mice showed that GC treatment alone does not produce

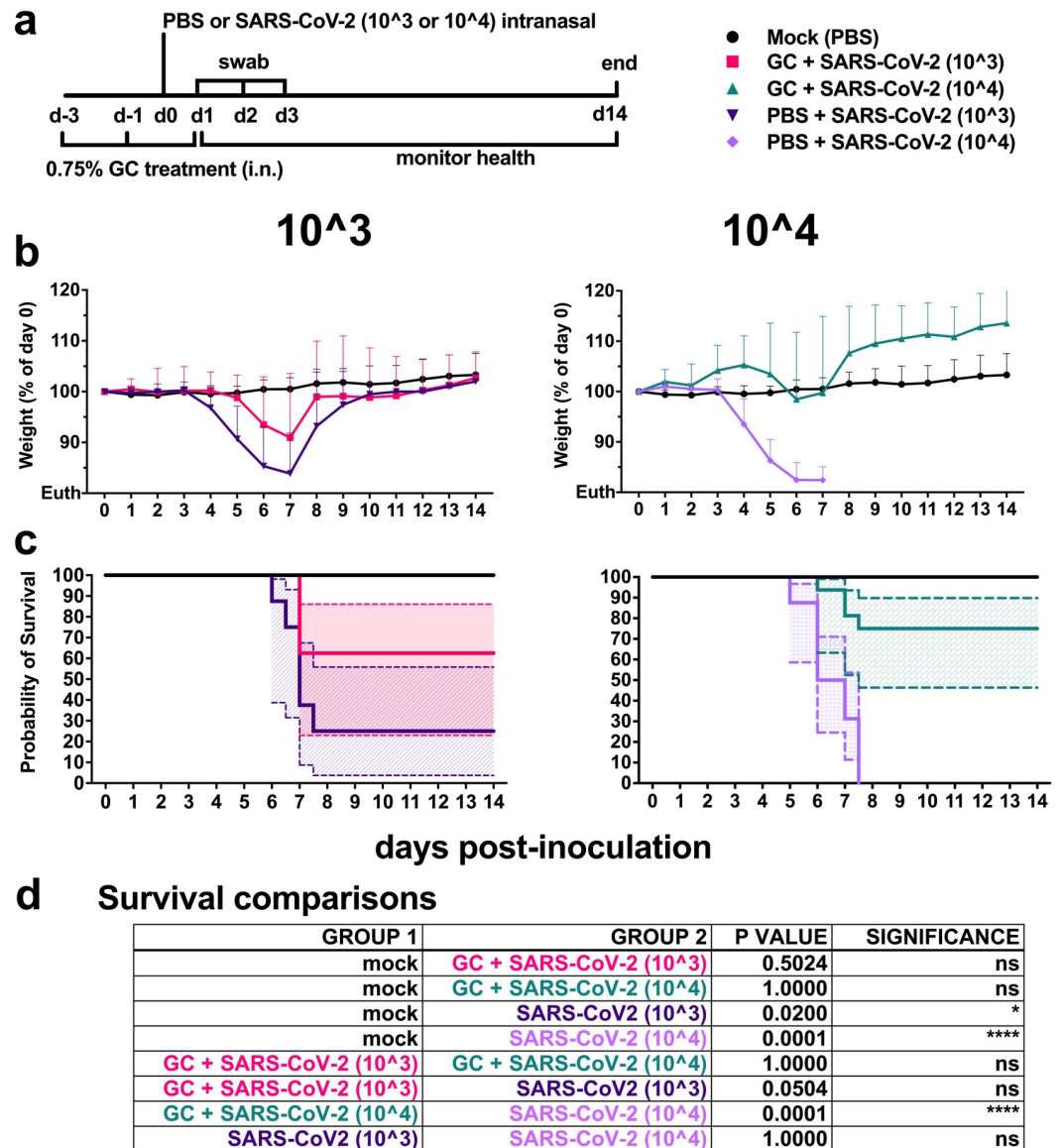


**Fig 1. N-dihydrogalactochitosan protects mice from SARS-CoV-2 mortality.** (a) **Experimental design** where 6-week-old male and female hACE2 transgenic mice were treated with 0.75% GC or PBS delivery vehicle at days -3, -1 and +1 post-inoculation. Mice were inoculated at day 0 with 103 or 104 PFU of SARS-CoV-2 or PBS (mock). Animals were weighed daily, and throats were swabbed on days 1 through 3. (b) **Weight** represented as a percentage of individual mouse weight at the time of inoculation. A main effect only model two-way ANOVA with Tukey corrected multiple comparisons yielded an  $F = 52.80$ ,  $p < 0.0001$ , 4 degrees of freedom. Each symbol represents an individual mouse, and the horizontal lines show geometric mean and error bars are geometric standard deviation. (c) **Survival proportions.** The solid lines are survival proportions, and the shaded boxes show 95% confidence intervals. (d) **Logrank Mantel-Cox comparisons of survival proportions** with Bonferroni corrected p-values, multiple pairwise tests, 1 degree of freedom.  $n = 8-16$  per group, 2 combined experiments.

<https://doi.org/10.1371/journal.pone.0289139.g001>

adverse clinical signs or pulmonary lesions. Lung histologic scores in mice administered GC were not significantly different from mice treated with PBS (S1 Fig and S1 Table in [S1 File](#)). Mice were inoculated i.n. 1 day prior to the final GC treatment with  $10^3$  or  $10^4$  plaque forming units (PFU) of SARS-CoV-2, a route and dose intended to produce high lethality in this model. Inocula were back-titrated to verify the administered dose. Tracheal swabs were collected for the first 3 days post inoculation and animals were monitored daily until day 14 for weight loss and health status.

Weight remained stable for the first 3 days in all groups. Weight in infected mice that were not GC-treated rapidly declined, starting at day 4 in the  $10^4$  PFU group, and at day 5 in the  $10^3$  PFU groups ([Fig 1b](#)). Half of the GC-treated mice administered  $10^4$  PFU experienced no weight loss throughout the duration of the study (S2 Fig in [S1 File](#)); conversely, their growth outpaced mock-infected counterparts treated with saline alone ( $p < 0.0001$ ). This effect was not limited to one biological sex and did not correlate with mouse starting weight at the time of study initiation. Additional mice lost weight starting at day 4 but did not reach euthanasia criteria (loss of 20% of initial body weight) and recovered to starting weight by day 10 post-inoculation. Relative to the  $10^4$  group, mice inoculated with  $10^3$  PFU SARS-CoV-2 exhibited delayed or transient weight loss, with 2 mice experiencing no weight loss over the duration of the study. At the higher inoculation dose of  $10^4$  PFU, GC significantly reduced weight loss versus delivery vehicle treated controls ( $p < 0.0001$ ). At the lower  $10^3$  PFU inoculation dose, GC trended toward protection from weight loss, which was confounded by non-uniform disease in delivery vehicle treated controls ( $p = 0.11$ ). Mice treated with delivery vehicle and inoculated with  $10^3$  or  $10^4$  PFU had a median survival time of  $7 \pm 3.3$  and  $6.5 \pm 0.9$  days, respectively ([Fig 1c](#)). At the lower inoculation dose of  $10^3$  PFU, GC had an efficacy of 37.5% protection from mortality ( $p = 0.05$ ) ([Fig 1c](#)). At the higher inoculation dose of  $10^4$  PFU, GC reduced SARS-CoV-2 mortality by 75% ( $p < 0.0001$ ) ([Fig 1d](#)). Together, these results demonstrate the potent efficacy of GC in preventing fatal SARS-CoV-2 disease in transgenic mice.

### N-dihydrogalactochitosan reduces SARS-CoV-2 viral levels in the respiratory tract

We next sought to determine whether GC reduced viral levels in addition to protecting mice from mortality. Infectious SARS-CoV-2 levels were assessed longitudinally in mice by swabbing throats from day 1 to 3 post-inoculation ([Fig 2a](#)). SARS-CoV-2 was detectable in tracheal swabs of infected animals at day 1 post inoculation and most animals had no detectible virus by day 3. Virus levels were elevated in mice inoculated with  $10^4$  PFU versus  $10^3$  PFU at 1 day post inoculation ( $p = 0.05$ ), but differences between inoculation doses were not detected after day 2 ( $p > 0.99$ ). GC significantly reduced virus levels in tracheal swabs at day 1 and day 2 post inoculation with  $10^4$  PFU ( $p = 0.0005$  and  $p = 0.02$ , respectively). A similar effect was not observed in mice that received the lower inoculum of  $10^3$  PFU. All delivery vehicle-treated mice had detectible virus in tracheal swabs following infection, while 29% (7/24) of GC-treated mice had no infectious virus isolated between days 1 and 3. Positive virus detection in tracheal swabs was not correlated with lethal disease in mice ( $p = 0.62$ , Fisher's exact test). Cumulative virus levels in tracheal swabs were calculated as area under the curve for individual animals ([Fig 2b](#)). GC significantly reduced the total shed virus levels in tracheal swabs in mice inoculated with  $10^4$  PFU from a geometric mean of 225 to 5.6 PFU ( $p < 0.0001$ ) and trended toward a reduction in animals inoculated with  $10^3$  PFU from 138 to 15 PFU ( $p = 0.08$ ).

As individual animals met humane experimental endpoints, mice were euthanized. Infectious virus levels were measured in the lungs ([Fig 2c](#)) and brain ([Fig 2d](#)) from mice on days 6, 7, and 14. Although mean virus levels were not significantly different, GC treatment trended

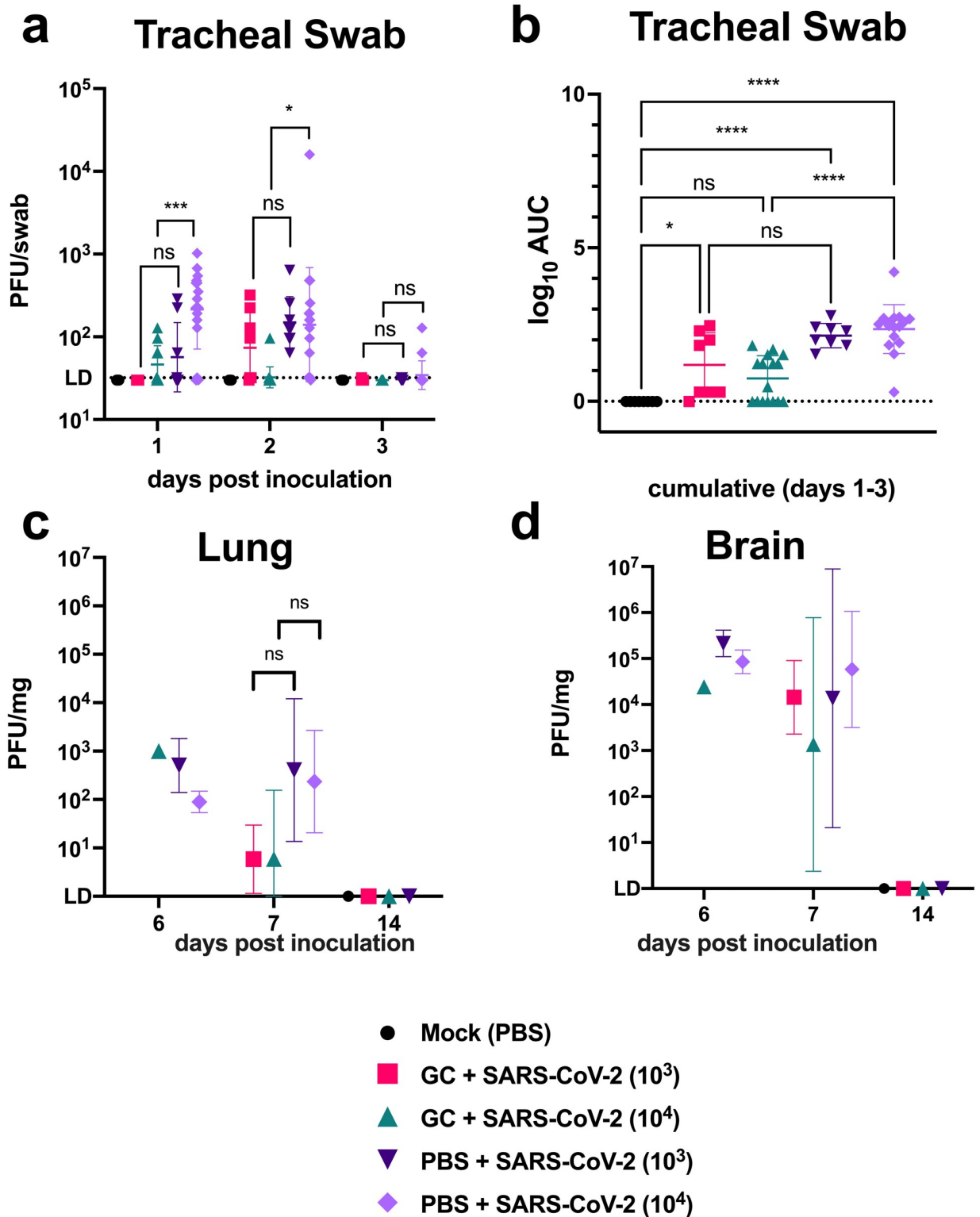


**Fig 2. N-dihydrogalactochitosan reduces SARS-CoV-2 detection in the respiratory tract.** Infectious SARS-CoV-2 was measured in (a) tracheal swabs collected from hACE2 transgenic mice on days 1, 2 and 3 post inoculation. Repeated measures two-way ANOVA with Tukey corrected multiple comparisons on log<sub>10</sub>-transformed values,  $F = 16.96, p < 0.0001, 4$  degrees of freedom. (b) Total area under the curve shows cumulative virus levels in swabs. ANOVA of log<sub>10</sub>-transformed total peak area with Tukey corrected multiple comparisons,  $F = 7.538, p < 0.0001, 4$  degrees of freedom. Mice were necropsied on days 6, 7 and 14 post-inoculation as euthanasia criteria were met. Infectious virus levels were

measured in (c) **lung** and (d) **brain** at experimental endpoints. Main effects only model two-way ANOVA on log<sub>10</sub>-transformed values,  $F = 2.431$ ,  $p = 0.0606$ , 4 degrees of freedom for lung,  $F = 0.8134$ ,  $p = 0.5229$ , 4 degrees of freedom for brain. Symbols are individual animals, horizontal lines show geometric mean, and error bars represent geometric standard deviation.  $n = 8$ – $16$  per group, 2 combined experiments. LD = limit of detection, AUC = area under the curve. \*  $p < 0.05$ , \*\*\*  $p < 0.001$ , \*\*\*\*  $p < 0.0001$ .

<https://doi.org/10.1371/journal.pone.0289139.g002>

toward reducing lung virus levels ( $F = 2.431$ ,  $p = 0.06$ , two-way ANOVA) with cumulative effects in animals inoculated with  $10^3$  PFU driving the main treatment effect ( $p = 0.06$ ).

Comparatively high viral titers were observed in the brain at the time of death, consistent with previous descriptions in this model [13]. Virus was detectible in the brain in all but 2 infected animals at the time of death, indicating neuroinvasion as a likely cause of morbidity. No significant differences in brain virus levels were observed between treatments ( $F = 0.8134$ ,  $p = 0.52$ , two-way ANOVA). No infectious virus was detectible in the lungs or brains of animals euthanized at day 14 post inoculation.

### N-dihydrogalactochitosan reduces the severity of histopathologic lesions associated with SARS-CoV-2 infection in lungs

Intranasal inoculation of hACE2 transgenic mice with PBS followed by mock inoculation resulted in normal lung architecture in most mice, although several animals exhibited mild alveolar septal inflammation, likely associated with i.n. administration (Fig 3a). By contrast, mice inoculated with  $10^3$  or  $10^4$  PFU SARS-CoV-2 (Fig 3c, representative  $10^3$  image shown) exhibited extensive lymphohistiocytic interstitial pneumonia with a peribronchiolar and perivascular distribution and scattered multinucleated syncytial cells 7 days post inoculation. Bronchiolitis, bronchiolar epithelial and alveolar septal necrosis, hemorrhage, fibrin, edema, and vascular endothelial inflammation were also occasionally noted. SARS-CoV-2-infected mice treated with GC showed lesser histopathologic lesions in the lung (Fig 3b, representative  $10^3$  image shown) compared to animals that did not receive GC, and inflammation was focally distributed instead of widespread. To quantify histopathologic changes, lung lesion severity was scored using specific criteria (S2 Table in S1 File). The percent of the lung that was affected in mice euthanized at 6, 7, or 14 days post inoculation as assessed by image analysis software did not differ significantly between SARS-CoV-2 infected mice treated with GC versus those who were not GC treated (Fig 3d). Despite this, GC treatment significantly reduced the mean lung histopathology severity score across all euthanasia days (although not when the results at days 6 and 7 or 14 were analyzed separately [Fig 3e]) for mice dosed with  $10^4$  PFU SARS-CoV-2; scores were reduced from 4.6 to 2.5 (ANOVA,  $p < 0.0001$ ) (Fig 3f). Mean scores for mice treated with GC and  $10^3$  PFU of SARS-CoV-2 trended towards being lower than for mice who did not receive GC but were not significantly different ( $p > 0.05$ ). Together, these data show that GC reduces SARS-CoV-2-induced disease in the lung of hACE2 mice, although only significantly in mice administered the higher  $10^4$  PFU dose of SARS-CoV-2.

### Mice treated with N-dihydrogalactochitosan produce neutralizing antibodies after SARS-CoV-2 exposure

We next sought to determine whether mice surviving SARS-CoV-2 inoculation produced a humoral immune response that might protect them from future infection. Serum from blood collected at day 14 post inoculation was assessed for neutralizing antibody against the inoculation strain of SARS-CoV-2 by plaque reduction neutralization test (PRNT) at the 80%



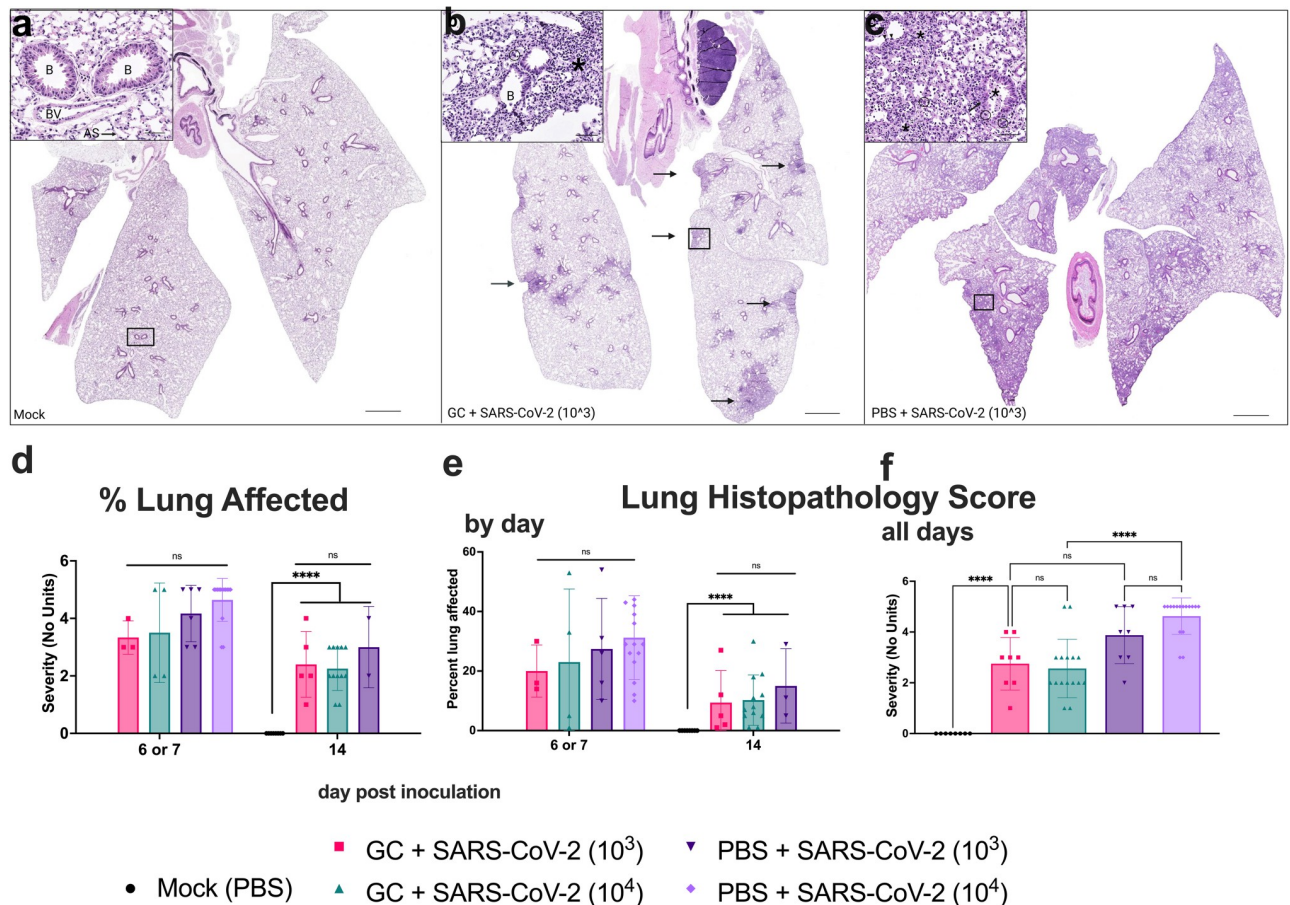


**Fig 3. N-dihydrogalactochitosan reduces histopathology associated with SARS-CoV-2 infection in lungs.** Lungs from hACE2 transgenic mice were collected at the time of death, thin sectioned, and hematoxylin and eosin stained for histopathological scoring. Images show representative lungs. (a) Normal lung from a PBS-treated, mock inoculated mouse at day 14. Bronchioles lined by epithelial cells, alveolar septa containing pulmonary capillaries lined by pneumocytes, and a small arteriole are visible (inset). (b) Lung from a GC + 10<sup>3</sup> PFU SARS-CoV-2 mouse at day 7 with patchy inflammation (black arrows) distributed around airways and affecting approximately 15% of the section. Peribronchiolar alveolar septal inflammation composed primarily of lymphocytes and macrophages (asterisk, inset) with scattered multinucleated cells. (c) Lung from a PBS + 10<sup>3</sup> PFU SARS-CoV-2 inoculated mouse at day 7 showing widespread, multifocal to coalescing inflammation affecting all lung lobes and approximately 60% of the section. The inset shows lymphohistiocytic bronchoalveolar inflammation (asterisk) with multinucleated syncytial cells (circled), endotheliitis (black arrowheads) and bronchiolar epithelial hyperplasia characterized by disorganization and piling-up of bronchiolar epithelium with increased mitotic figures (black arrows). (d) Total affected lung area was estimated using image analysis software. (e-f) Lung lesion severity was scored according to criteria defined in S2 Table in S1 File. Scale bars are 2 mm (subgross) and 50  $\mu$ m (insets). As = alveolar septa, B = bronchioles, Br = bronchus, BV = blood vessel. \*\*  $p < 0.01$ , \*\*\*  $p < 0.001$ , \*\*\*\*  $p < 0.0001$ , ns = not significant. ANOVA,  $F = 35.86$ ,  $p < 0.0001$ , 4 degrees of freedom (e). ANOVA,  $F = 10.32$ ,  $p < 0.0001$ , 4 degrees of freedom (f). Symbols are individual animals, bars show the mean, and error bars show the standard deviation,  $n = 8-16$  per group, 2 combined experiments.

<https://doi.org/10.1371/journal.pone.0289139.g003>

neutralization threshold (Fig 4). All mice surviving virus inoculation generated neutralizing antibodies. Mice in the GC group inoculated with 10<sup>3</sup> or 10<sup>4</sup> PFU generated neutralizing titers of 1:676 and 1:861 (geometric mean), respectively. In comparison, PBS-administered mice that received an inoculation dose of 10<sup>3</sup> PFU had a mean neutralizing titer of 1:1448. Neutralizing antibody titers were not different across treatments ( $p > 0.99$ ) or virus dose, although PBS-administered mice inoculated with 10<sup>4</sup> PFU SARS-CoV-2 were unavailable for comparison due to uniform lethality. These data confirm that surviving mice were infected and indicate that all SARS-CoV-2 inoculated animals, regardless of treatment, were able to develop adaptive immune responses that could potentially protect against reinfection.

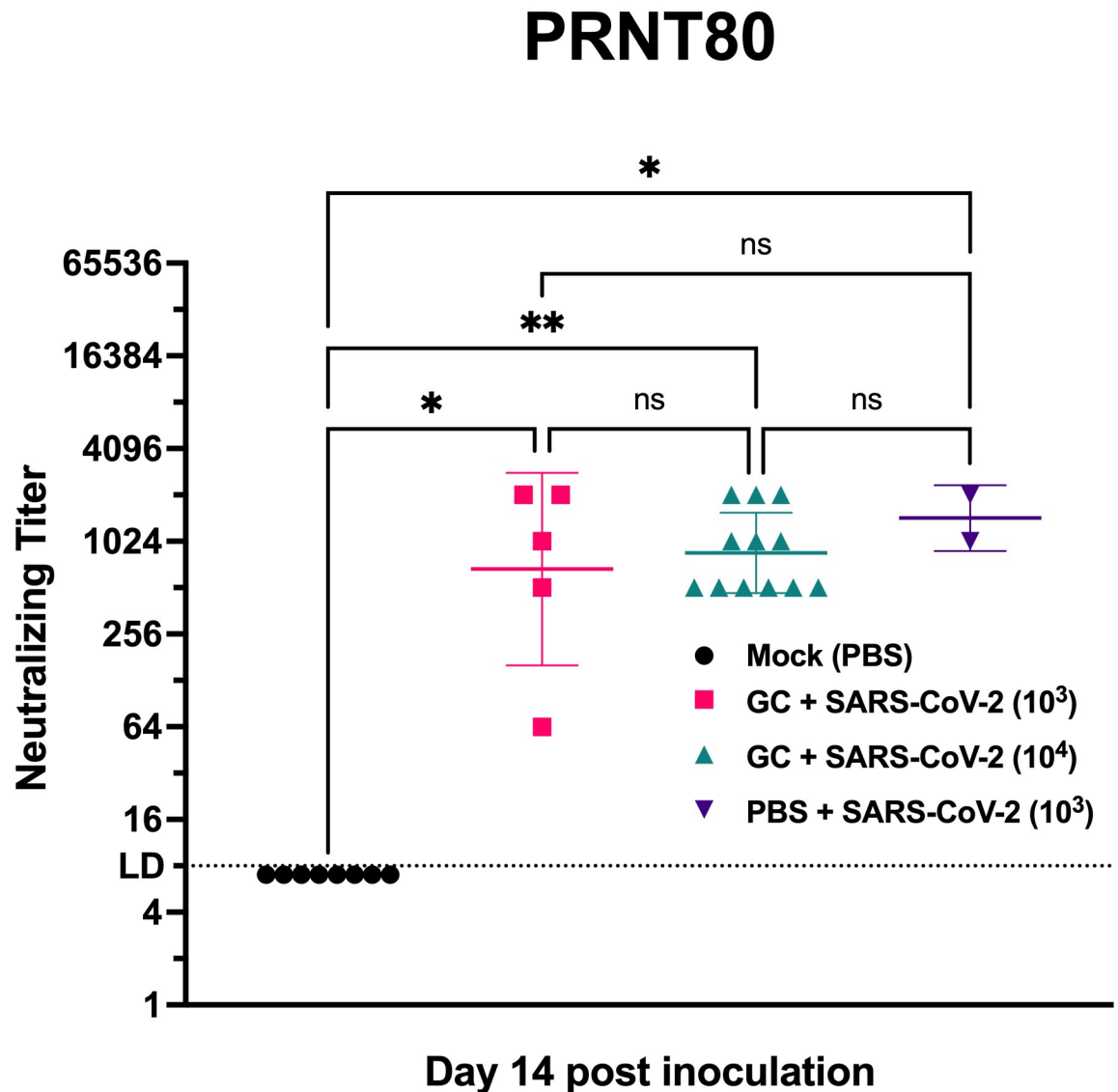


**Fig 4. N-dihydrogalactochitosan treated mice surviving SARS-CoV-2 inoculation produce neutralizing antibodies.** Neutralizing antibody was assessed by 80% plaque reduction neutralization test (PRNT80) in serum from hACE2 transgenic mice surviving to day 14 post inoculation. No PBS treated mice inoculated with  $10^4$  PFU SARS-CoV-2 were available for comparison due to uniform mortality. \*  $p < 0.05$ , \*\*  $p < 0.01$ , LD = limit of detection. Kruskal-Wallis test with Dunn corrected multiple comparisons,  $H = 17.87$ ,  $p = 0.0005$ , 3 degrees of freedom. Symbols are individual animals, horizontal lines are geometric mean and error bars show geometric standard deviation,  $n = 2-12$  per group, two combined experiments.

<https://doi.org/10.1371/journal.pone.0289139.g004>

### Fluorescent labeled N-dihydrogalactochitosan administered intranasally in mice localizes to the mucous of the nasal cavity

Finally, we administered fluorescent labeled GC (FITC-GC) i.n. to mice to examine retention kinetics in the nasal concha. Two mice per time point were FITC-GC treated once and then euthanized 2h, 9h, or 2d later, or were treated twice (2X) and harvested 3d later; for these mice, the second treatment was administered 1 day before euthanasia. Negative control mice were not administered FITC-GC. Histopathology was evaluated and quantified using a scoring rubric developed for the nasal cavity (S3 Table in S1 File). Fluorescence in the nasal cavity was

visualized with microscopy measured by calculating the percent area of the total nasal conchae per slide with a fluorescent signal. Fluorescing aggregates identified within the oral cavity of several treated mice were not included in the measurements, as they were outside the nasal conchae. Negative control mice had no fluorescent foci (Fig 5a). For FITC-GC treated mice, fluorescing foci were predominantly within the lumen or loosely adhered to the nasal mucosa, with infrequent fluorescing areas within the epithelium (Fig 5b–5f). Although small group sizes preclude statistical assessments, the fluorescent signal of FITC-GC in the nasal cavity of all but 1 FITC-GC treated mouse appeared higher than in negative control mice (Fig 5g). Histologically, fluorescent material was typically associated with inflammatory cells, mucous, and debris. Histology scoring in the nasal concha of these mice showed that while PBS treated mice

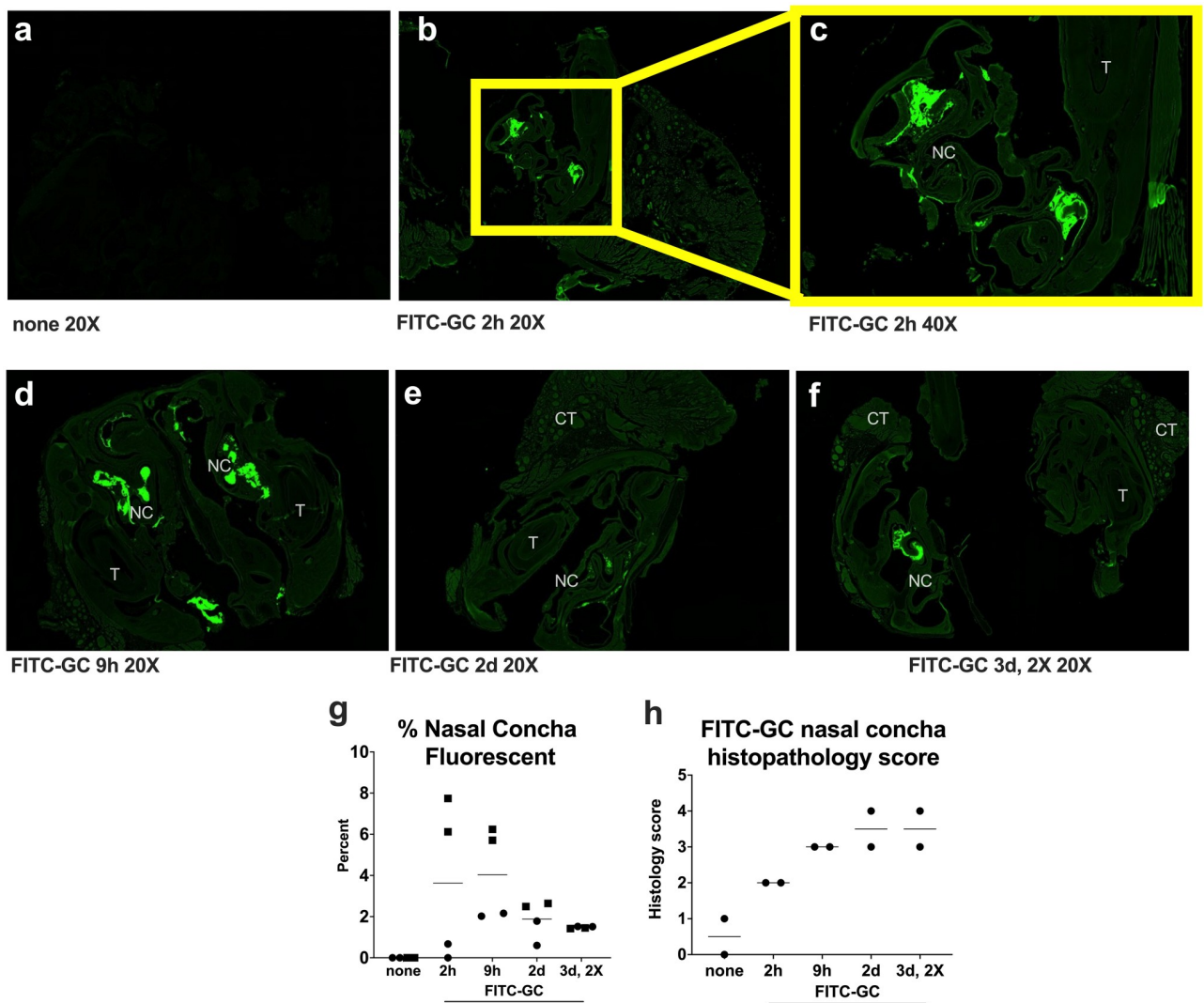


**Fig 5. Fluorescent labeled GC (FITC-GC) administered intranasally to mice localizes to the nasal cavity and immune cell influx results in nasal concha histopathology scores.** Fluorescent images of nasal concha from mice administered (a) no FITC-GC or (b–f) 0.75% FITC-GC i.n. administered once, and euthanized 2h, 9h, 2d or 3d later. Mice in the group euthanized 3d after the first treatment were administered a second treatment (2X) 1d before euthanasia. Panel (b) is at a magnification of 10X, (c–f) are at a magnification of 20X. NC is nasal conchae, T is tooth, CT is connective tissue. (g) Fluorescence measured as percent of total image area, limited to nasal mucosa. Matching symbols for each time show 2 measurements from the same mouse. (h) Nasal concha histopathology scores based on the scoring rubric in S3 Table in S1 File. N = 2 mice per time. The small group size precluded statistical assessments.

<https://doi.org/10.1371/journal.pone.0289139.g005>

had low scores, FITC-GC treatment increased scores (Fig 5h). Treatment of the group of mice euthanized 3d post treatment with 2 administrations of FITC-GC did not increase the percent nasal concha fluorescent or histology scores. All FITC-GC treated mice showed moderate rhinitis characterized by mixed inflammatory mucosal or submucosal infiltration and or nasal cavity exudate composed of neutrophils, macrophages, and lymphocytes and mild to moderate hemorrhage, fibrin, edema, and sometimes necrotic debris. Together, these data support a process whereby GC administered i.n. to mice remains confined to the superficial mucosa and acts as a mild irritant without eliciting deeper inflammation.

## Discussion

Intranasal administration of GC to prevent or treat SARS-CoV-2 represents a novel application of this potent immunostimulatory compound. In the present study, GC was well-tolerated and prevented lethal disease in up to 75% of treated humanized mice, while all mice not receiving GC but inoculated with  $10^4$  PFU SARS-CoV-2 required euthanasia. All surviving animals had neutralizing antibodies detectable at 14 days post inoculation. Similar SARS-CoV-2 antibody titers were detected in GC-treated and untreated animals. Mice that received GC treatment also displayed lower levels of infectious SARS-CoV-2 in tracheal swabs collected 1 to 2 days post inoculation. Reducing virus levels in the upper airway has gained particular significance as recent vaccine breakthrough cases with variants of concern demonstrate SARS-CoV-2 shedding at similar levels to unvaccinated individuals, which is a key determinant of transmission potential [52]. Our findings demonstrate a reduction in viral burden and virus-induced disease along with a resultant increase in survival due to GC treatment.

GC is a polymeric mixture containing strands of varying lengths of selectively galactose-conjugated and partially deacetylated  $\beta$ -0-4-linked N-acetylglucosamine molecules with a specific range of molecular weights [42,43,46,47]. Synthesized and purified under Good Manufacturing Practice (GMP) conditions, N-dihydrogalactochitosan is a well-characterized variant of GC. Characterization and quality control testing ruled out contamination from endotoxins, heavy metals, and other impurities, which eliminates a major confounding factor in the research of these naturally derived molecules, and of chitosan in particular [53]. Water solubility, immunological properties, biocompatibility, and a favorable toxicity profile are key features of GC. The unconjugated base polymer, chitin, is a primary structural component of cell walls for organisms ranging from fungi to arthropods [24]. Chitosan, a derivative of chitin, is deacetylated through alkaline treatment and is marketed as a nutritional supplement [54] and used as a biopolymer [55]. Unmodified chitosan has been used successfully to treat influenza A virus infection in mice [32], demonstrating a potential application as a non-specific antiviral compound for respiratory virus infection. However, unmodified chitosan has low solubility in neutral buffered aqueous solution and requires acidic formulation; poor characterization, purification and lack of controlled synthetic pathways lead to poor reproducibility and unpredictable outcomes [53]. GC circumvents these limitations through a controlled and reproducible process of synthetically attaching galactose to the free-amino groups of the chitosan base, improving solubility (and thus bioavailability) while maintaining a physiological pH. GC has been previously used as a combination anti-tumor therapy due to its immunoadjuvant properties [48,50], but its utility as a broad-acting antiviral compound has not previously been investigated.

Immunoadjuvants stimulate non-specific innate immune responses through various mechanisms. Some use pattern-recognition receptors, including the Toll-like receptor (TLR) family of antigen detection complexes. While the mechanism of SARS-CoV-2 protection has not been determined for GC, chitosan, and similar polymers of N-acetylglucosamine, interact with

TLR2, which serves as a rationale for inclusion of chitosan as a vaccine adjuvant. TLR2 signals through myeloid differentiation factor 88 (MyD88) to stimulate the nuclear factor kappa B (NF- $\kappa$ B) pathway and downstream inflammatory and anti-microbial cytokine responses [56,57]. TLR engagement of the canonical NF- $\kappa$ B pathway up-regulates both tumor necrosis factor alpha (TNF- $\alpha$ ) and interleukin-6 (IL-6), two potent pro-inflammatory effectors. IL-6, which is necessary for antiviral immunity against other virus families, has been identified as a target of dysregulation associated with hyperinflammatory responses in the lungs during SARS-family coronavirus infections. SARS-CoV-1 nucleocapsid protein can stimulate NF- $\kappa$ B activation and IL-6 production independent of infection [58]. Prolonged high levels of IL-6 are correlated with severe COVID-19 outcomes in humans, and a similar association has been found in ferrets infected with SARS-CoV-2 [59]. The timing of IL-6 production may play a critical role in determining whether viral clearance is achieved or alternatively, hyperinflammatory responses result. Early, but not late, induction of IL-6 during respiratory syncytial virus (RSV), influenza A, and rhinovirus infections promote viral clearance and limit prolonged inflammation by establishing regulatory T cell populations that limit virus spread [60]. Similarly, timed induction of pro-inflammatory responses by GC treatment pre- and post-infection may promote viral clearance before virus-mediated dysregulation of this pathway can occur. As such, future studies should explore the timing of GC treatment and regulation of IL-6 and associated pro-inflammatory pathways.

The data in this study demonstrate that treatment with GC does not impact development of a neutralizing antibody response by day 14 after SARS-CoV-2 inoculation, even though it reduced infectious SARS-CoV-2 in tracheal swabs. These data suggest GC functions as an immunoadjuvant that can modulate innate immune responses after SARS-CoV-2 infection, leading to stimulation of robust antiviral adaptive immunity. Experimental evidence from cell culture and animal models supports at least four mechanisms by which complex carbohydrates such as GC could stimulate the innate and adaptive immune systems [61–64]. First, GC recognition by sensors on macrophages and dendritic cells (DC) can stimulate innate immune defenses [65–67]. While immune receptors for GC have not been identified, chitosan binding to C-type lectin receptors such as dectin-1 can initiate innate immune signaling [68,69]. Second, GC-mediated antigen uptake [70] and antigen presentation by DCs could lead to CD4 and CD8 T cell responses [47,48]. Studies in mice show GC induces type 1 IFN [50], leading to enhanced DC activation and robust CD4 T helper cells [62]. Activation of the STING pathway by type I IFN is a known important antiviral pathway independent of neutralizing antibodies [51]. Notably, DNA sensor activation is mediated by chitosan-induced cellular DNA release. Third, physical antigen sequestration and slow antigen release within draining lymph nodes facilitated by GC could potentially prolong germinal center reactions, thereby enhancing humoral immunity by fostering affinity maturation of B cells [71,72]. Fourth, GC triggers recruitment of neutrophils, macrophages, and lymphocytes in the nasal cavity indicating a heightened innate immune response that could eliminate SARS-CoV-2 or other respiratory pathogens and infected cells at the entry site via mechanisms such as phagocytosis, formation of neutrophil extracellular traps, the release of reactive oxygen species, and inflammatory cytokines such as IL-1 $\beta$  and TNF $\alpha$ , that recruit more leukocytes. Thus, GC may have potential as a dual-purpose preventative and therapeutic with immunostimulatory properties. Future studies are needed to investigate the impact of GC on SARS-CoV-2-specific immune responses.

In addition to the immunoadjuvant properties of GC, direct interactions between GC and SARS-CoV-2 in the nasal cavity may contribute to the protection we observed in mice. As the nasopharyngeal and oral cavity are often the primary entry sites of SARS-CoV-2 and other respiratory viruses, interventions or medications at these locations could provide an important boost in the first line of defense. The reduction in SARS-CoV-2 levels in GC treated mice in

the first 2 days post-inoculation suggests that GC has early effects that hamper the initial phase of viral infection, especially given that serum neutralizing antibodies are not detectable before about 7 days. Although we observed that GC reduced tracheal swab titers, we acknowledge that tracheal swabs may less accurately represent virus levels in the upper respiratory tract compared to nasal turbinates. Additionally, GC is viscous, and its cationic charge allows it to bind to negatively charged biomolecules such as mucin and act as a mucoadhesive. Our labeling studies with FITC-GC show it remains in the nasal cavity after intranasal administration. GC present at the time of infection may therefore act as a physical barrier and/or directly inactivate SARS-CoV-2 before it can initiate infection. Additional studies of the temporal kinetics of GC bioavailability and detailed studies of GC-virus interactions to establish whether GC blocks virus entry and/or replication are needed to establish mechanisms of protection; these experiments could also clarify why greater protection from lethal disease was observed after inoculation with the higher SARS-CoV-2 dose in these studies.

In terms of safety, in animal model studies [73] or human clinical trials for treating tumors [74,75], GC has not elicited autoimmune-like disease or pathology. Even so, future work should involve additional GC safety studies in animal models with enhanced inflammatory reactions including autoimmune diseases or allergic reactions such as asthma or generation of auto-antibodies.

Although it may have clinical applications for treating infectious diseases in the future (reviewed in [76]), to our knowledge, there is currently no evidence to support the antiviral properties of chitosan and its derivatives from human studies. Available research on antiviral activity of chitosan comes from *in vitro* studies or animal models. In addition to inhibition of influenza virus by chitosan [33], other studies (reviewed in [24]) show the potential utility of chitosan across a broad spectrum of infectious agents, extending to phage and virus infections in plants and animals, albeit acknowledging that its antiviral mechanisms are not understood. More recently, other studies have also explored the use of chitosan and derivatives against SARS-CoV-2, and although chitosan has not been tested for a breadth of activity against a broad range of viruses, other studies speculate that the chitosan compound family may exert broad antiviral properties [37,77]. A recent review [78] covered the uses of chitosan and derivatives, exploring in detail some of the compound alterations that boost antimicrobial potential. The spectrum of potential applications noted is particularly broad, and includes antibacterial, antifungal as well as antiviral, (including influenza and potentially other respiratory viruses), and anticancer opportunities. Furthermore, chitosan may be coupled with antiviral composites to produce synergistic effects. A study by Pyrc *et al.* [36] in 2021 describes the application of a chitosan derivative administered as a nasal spray in the same transgenic mice we used; however, only limited effectiveness was demonstrated, suggesting that not all chitosan variants are equal and supporting a role for chitosan in a therapeutic that consists of a combination of compounds.

In summary, we show here that GC treatment of humanized mice pre- and post-infection with SARS-CoV-2 reduces lethal disease, virus levels in the upper respiratory tract, and significant lesions in the lungs. These data suggest a possible role of GC as a SARS-CoV-2 countermeasure. Additional pre-clinical studies could focus on the mechanism of protection, including further assessment of the antiviral and immunomodulatory effects of GC. We acknowledge that a limitation of this study is that GC was administered both before and after SARS-CoV-2 exposure, which prevents evaluation of the impact of the timing of GC administration on disease outcome. Future studies should determine optimal GC dose and schedule that would confer the greatest benefit in reducing disease, as well as to assess whether GC confers both prophylactic and therapeutic benefits in mice that are euthanized at pre-determined intervals instead of when they meet euthanasia criteria. Future studies should also explore

localization of GC in areas outside of the nasal cavity, as well as pharmacokinetics and metabolism. Clinical application of GC could be enhanced with future studies showing prophylactic and therapeutic benefits for other common respiratory viruses like influenza virus, respiratory syncytial virus, human parainfluenza virus, and other non-SARS-CoV-2 coronaviruses.

## Methods

### Ethics statement

Mouse work was conducted on protocols #21868 (University of California, Davis), # R20-026 (University of Oklahoma) and # AUP007 (Immunophotonics). Each institutional animal care and use committee (IACUC) approved all mouse work. Infectious virus was handled in certified animal biosafety level 3 laboratory (ABSL-3) spaces in compliance with approved institutional biological use authorization #R2813 at the University of California, Davis. The University of California, Davis, is accredited by the Association for Assessment and Accreditation of Laboratory Animal Care (AAALAC). All mouse work adhered to the NIH Guide for the Care and Use of Laboratory Animals [79].

### Mice

Equal numbers of male and female transgenic mice expressing the human ACE2 receptor on a K18 transgene in a C57Bl/6J background (B6.Cg-Tg(K18-ACE2)2Prln/J, referenced as 'hACE2') were purchased at 5 weeks of age from Jackson Laboratories (Sacramento, CA) and acclimated for up to 6 days. C57Bl/6 mice treated with fluorescent GC were used at 6–8 weeks of age and were purchased from Jackson Laboratories. Mice for SARS-CoV-2 studies were co-housed by sex in ABSL-3 conditions. At all 3 institutions, mice were housed in groups of up to 4 animals per cage at 22–25°C and a 12:12 hour light: dark cycle. Rodent chow with 18% protein content and sterile bottled water was provided *ad libitum* for the duration of experiments.

### Virus

SARS-CoV-2/human/USA/CA-CZB-59X002/2020 (GenBank #MT394528), which was isolated from a patient in 2020 in Northern California and passaged once in Vero-E6 cells, was generously provided by Dr. Christopher Miller (University of California, Davis). To generate stocks for these studies, SARS-CoV-2 was passaged one additional time in Vero-E6 cells to achieve a titer of  $2.2 \times 10^7$  plaque forming units (PFU)/mL. Single-use virus aliquots were stored at -80°C.

### N-dihydrogalactochitosan treatment

Sterile 1% weight/volume N-dihydrogalactochitosan (GC) was provided by Immunophotonics. GC was generated using Good Manufacturing Practices (GMP). Testing of GC included appearance, identity (1H NMR and UV/Vis), assay (HPLC), degree of galactation (1H NMR), viscosity, specific gravity, pH, microbiological (endotoxins and sterility), subvisible particulate matter, impurities (boron, galactose, galactitol, transition metals), molecular weight, and polydispersity indices. GC was presented as a 1.0% sterile solution (10 mg/ml) in 5 ml sealed vials and was diluted with sterile deionized water and sterile filtered 20X phosphate buffered saline (PBS) to a final concentration of 0.75% GC and 1X PBS. Mice were anesthetized with isoflurane and 40 µL of either diluted GC or PBS delivery vehicle was administered intranasally (i.n.) by a hanging drop over both nares. Mice were treated identically at 3 days and 1 day prior to inoculation and 1 day post inoculation. Six-week-old male (N = 7) and female (N = 7) mice were used to assess the histopathologic effects of GC on the murine lung.

Mice were treated on the same schedule as above, and a subset were euthanized 2 or 14 days after the last treatment. Cumulative lung lesion scores were determined using a scoring scale (S2 Table in [S1 File](#)).

### SARS-CoV-2 inoculation

At inoculation, mice were anesthetized and administered 30  $\mu\text{L}$  of PBS or SARS-CoV-2 diluted in PBS at a dose of  $10^3$  or  $10^4$  PFU i.n. via hanging drop. Inocula were back-titrated to confirm the target dose. Mice were monitored twice daily for changes in weight, ruffled fur, ataxia, and labored breathing for up to 14 days. On days 1, 2, and 3, mice were anesthetized with isoflurane and throats were swabbed with rayon-tipped swabs (Puritan, Fisher Scientific, Fisher Scientific, Waltham, MA). The process for swabbing was constant across all treatment groups. Swabs were vortexed briefly in 400  $\mu\text{L}$  of Dulbecco's Modified Eagles Medium (DMEM, Fisher Scientific, Waltham, MA) and frozen at  $-80^\circ\text{C}$ . Mice were euthanized prior to experimental endpoint if weight loss exceeded 20% of the starting weight or if animals were deemed moribund as evidenced by limb weakness, ataxia or dragging of limbs, loss of limb function or rapid or depressed respiration rate. An adverse event was defined as any moribund disease signs at any time over the duration of the experiment. Prior to euthanasia, whole blood was collected by submandibular vein puncture under isoflurane anesthesia. Whole blood was clotted for  $>10$  min at room temperature then centrifuged for 5 minutes at  $8,000 \times g$  and cleared serum was stored at  $-80^\circ\text{C}$ . Mice were euthanized by isoflurane overdose and cervical dislocation then perfused with cold sterile PBS. Lung (right inferior lobe) and brain (left hemisphere) were weighed and homogenized in 1–10  $\mu\text{L}/\text{mg}$  DMEM with a sterile glass bead at 30 Hz for 4 minutes using a TissueLyser (Qiagen, Germantown, MD) automated homogenizer. Homogenates were cleared by centrifugation at  $10,000 \times g$  for 4 minutes and the cleared fraction was stored at  $-80^\circ\text{C}$ .

### Histopathology

At necropsy, lungs were inflated with 10% buffered formalin (Fisher Scientific, Waltham, MA) and mice were fixed for 48 hours at room temperature in a 10-fold volume of 10% buffered formalin. Skulls were demineralized in a 10-fold volume of 0.5 M ethylenediamine tetraacetic acid (EDTA) (pH = 7) at  $4^\circ\text{C}$  for 14 days, with EDTA solution exchanges every 3 days. Tissues were embedded in paraffin, thin-sectioned, and stained with hematoxylin and eosin (H&E). H&E-stained slides were scanned by a whole-slide image technique using an Aperio slide scanner (Leica, Buffalo Grove, IL) with a resolution of  $0.24 \mu\text{m}/\text{pixel}$ . Image files were uploaded on a Leica hosted web-based site and a board certified veterinary anatomic pathologist without knowledge of treatment conditions evaluated sections for SARS-CoV-2 induced histologic lesions. For quantitative assessment of lung inflammation, digital images were captured and analyzed using ImageJ software (Fiji, NIH) to estimate the area of inflamed tissue that was visible to the naked eye at subgross magnification as a percentage of the total surface area of the lung section. Each lung section was scored as described (S2 Table in [S1 File](#)).

### Fluorescent labeled tracing of GC in the nasal cavity

FITC-labeled GC at a concentration of 0.75% (7.5 mg/ml) was applied i.n. in 40  $\mu\text{L}$  to female and male wildtype C57BL/6 mice aged 6–8 weeks (Jackson Laboratories). FITC-GC was manufactured by Immunophotonics, LLC. At 2h, 9h, 2d and 3d (where the last group was administered FITC-GC one additional time 1d before euthanasia) after application, 2 mice per time were euthanized. Two additional mice were not FITC-GC treated; these served as negative controls. The anterior half of the cranium was harvested as described [80] and placed into 4%



paraformaldehyde (Cat. 157-8-100, Electron Microscopy Sciences) for 24h at room temperature. Samples were sent to the St. Louis University (SLU) histology core for processing. The samples were decalcified in ImmunoCal for 2 weeks with the solution changed every 3d. Next, they were washed with PBS then processed into paraffin and embedded. The sections were taken at 4.5  $\mu\text{m}$  every 200  $\mu\text{m}$ . The stained slides were scanned at 20X on an Olympus VS120 to detect the FITC signal. For the unstained slides that were scanned, they were first deparaffinized and then dehydrated so they could be coverslipped and scanned. Five  $\mu\text{m}$  sections were taken every 200  $\mu\text{m}$  and placed on a slide for examination under an epifluorescence microscope to detect the FITC signal. Nasal concha were evaluated histopathologically and measurements of fluorescence were performed using ImageJ (Fiji). Briefly, images were standardized using the FITC Green channel with rendering set to 1500 for optimal contrast. Screenshots of each micrograph were taken, and the total area of nasal cavity and mucosa was traced and recorded. Teeth, oral mucosa, and connective tissues were excluded for consistency, as sections were variably cut. Fluorescent foci were traced and recorded. The percent area affected was calculated for each slide as total fluorescent area divided by total nasal cavity area. Two sets of measurements were taken per individual, with 4 total observations per treatment since 2 mice were included in each treatment group.

### Plaque assay

Washes from tracheal swabs, serum, residual inocula, and lung and brain homogenates were thawed and assayed. Samples were serially diluted 10-fold in DMEM with 1% bovine serum albumen (BSA) starting at an initial dilution of 1:8. 125  $\mu\text{L}$  of each dilution was added to confluent Vero CCL-81 cells (ATCC, Manassas, VA) in 12-well plates with cell culture media decanted. Virus was incubated on cells for 1 hour at 5%  $\text{CO}_2$  in a humidified 37°C incubator. Cell monolayers were overlaid with 0.5% agarose dissolved in DMEM with 5% fetal bovine serum (FBS) and 1x antibiotic-antimycotic (Fisher Scientific, Waltham, MA) and incubated for 3d at 5%  $\text{CO}_2$  and 37°C in a humidified incubator. Cells were fixed for >30 minutes with 4% formaldehyde then agarose plugs were removed. Cells were stained with 0.05% crystal violet in 20% ethanol for 10 minutes then rinsed three times with water. Plates were inverted to dry completely and the number of plaques in each well was counted. Viral titers were recorded as the reciprocal of the highest dilution where plaques were noted and are represented as PFU per swab or PFU per mg of solid tissue.

### Plaque reduction neutralization test

Serum collected from mice at day 14 post inoculation was thawed at 37°C and 30  $\mu\text{L}$  was heated in a water bath for 30 minutes at 56°C to inactivate complement proteins. Serum was diluted 4-fold with virus diluent consisting of PBS and 1% FBS, then samples were serially 2-fold diluted 11 times for a dynamic range of 1:4 to 1:4096. An equal volume of virus diluent containing 80 PFU of SARS-CoV-2 was added to each antibody dilution and a no-antibody control consisting of virus diluent only, resulting in a final dynamic range of 1:4 to 1:8192 with one no-antibody control. Antibody-virus dilution series were incubated for 1 hour at 37°C after which they were applied to confluent Vero CCL-81 cells in single-replicate and incubated for 1 hour at 5%  $\text{CO}_2$  and 37°C in a humidified incubator. Cells were overlaid, incubated, fixed, and stained as described above for plaque assays. Neutralizing titer is defined as the reciprocal of the dilution for which fewer than 20% of plaques were detected versus the no-antibody control (>80% neutralization).

## Statistics

All statistical tests were performed with GraphPad PRISM 9.0.2 (GraphPad Software). Mann Whitney tests were used to compare cumulative pulmonary histologic lesion scores in GC or PBS treated mice. Logrank (Mantel-Cox) test for survival proportions were performed pairwise and *p*-values were adjusted with Bonferroni correction using R version 4.0.0 (R Project) `p.adjust` function. The correlation between mortality and positive virus detection was calculated by Fisher's exact test. Repeated measures two-way ANOVA tests were performed on  $\log_{10}$ -transformed viral titers and multiple comparisons were computed according to Tukey method. Main effect two-way ANOVA tests were performed on mouse weights normalized to starting values at the time of virus inoculation or  $\log_{10}$ -transformed viral titers and multiple comparisons were computed with Tukey's method. Area under the curve (AUC) was calculated for longitudinally collected tracheal swabs from days 1, 2, and 3 and  $\log_{10}$ -transformed. ANOVA of grouped  $\log_{10}$ -AUC was performed with multiple comparisons computed with Tukey's method. ANOVA was performed on untransformed histologic scores or percentage of lung affected by inflammation and multiple comparisons were computed with Bonferroni's method. A Kruskal-Wallis H test was performed on untransformed PRNT<sub>80</sub> neutralization values and multiple comparisons were computed according to Dunn's method.

## Supporting information

**S1 File. Contains all the supporting tables and figures.**  
(PDF)

## Author Contributions

**Conceptualization:** Christopher M. Weiss, Hongwei Liu, Ashley R. Hoover, Samuel Lam, Tomas Hode, Richard M. Levenson, Lark L. Coffey.

**Data curation:** Christopher M. Weiss.

**Funding acquisition:** Richard M. Levenson, Wei R. Chen, Lark L. Coffey.

**Investigation:** Christopher M. Weiss, Hongwei Liu, Erin E. Ball, Ashley R. Hoover, Talia S. Wong, Chun Fung Wong.

**Supervision:** Wei R. Chen, Lark L. Coffey.

**Validation:** Christopher M. Weiss.

**Visualization:** Christopher M. Weiss, Hongwei Liu, Erin E. Ball, M. Kevin Keel, Lark L. Coffey.

**Writing – original draft:** Christopher M. Weiss.

**Writing – review & editing:** Christopher M. Weiss, Hongwei Liu, Erin E. Ball, Ashley R. Hoover, Talia S. Wong, Chun Fung Wong, Samuel Lam, Tomas Hode, M. Kevin Keel, Richard M. Levenson, Wei R. Chen, Lark L. Coffey.

## References

1. Huang C, Wang Y, Li X, Ren L, Zhao J, Hu Y, et al. Clinical features of patients infected with 2019 novel coronavirus in Wuhan, China. *The Lancet*. 2020. [https://doi.org/10.1016/S0140-6736\(20\)30183-5](https://doi.org/10.1016/S0140-6736(20)30183-5) PMID: 31986264
2. COVID-19 Map—Johns Hopkins Coronavirus Resource Center. [cited 6 Mar 2023]. <https://coronavirus.jhu.edu/map.html>.

3. Wang D, Hu B, Hu C, Zhu F, Liu X, Zhang J, et al. Clinical Characteristics of 138 Hospitalized Patients with 2019 Novel Coronavirus-Infected Pneumonia in Wuhan, China. *JAMA—Journal of the American Medical Association*. 2020; 323: 1061–1069. <https://doi.org/10.1001/jama.2020.1585> PMID: [32031570](https://pubmed.ncbi.nlm.nih.gov/32031570/)
4. Chen N, Zhou M, Dong X, Qu J, Gong F, Han Y, et al. Epidemiological and clinical characteristics of 99 cases of 2019 novel coronavirus pneumonia in Wuhan, China: a descriptive study. *The Lancet*. 2020; 395: 507–513. [https://doi.org/10.1016/S0140-6736\(20\)30211-7](https://doi.org/10.1016/S0140-6736(20)30211-7) PMID: [32007143](https://pubmed.ncbi.nlm.nih.gov/32007143/)
5. Zhou F, Yu T, Du R, Fan G, Liu Y, Liu Z, et al. Clinical course and risk factors for mortality of adult inpatients with COVID-19 in Wuhan, China: a retrospective cohort study. *The Lancet*. 2020; 395: 1054–1062. [https://doi.org/10.1016/S0140-6736\(20\)30566-3](https://doi.org/10.1016/S0140-6736(20)30566-3) PMID: [32171076](https://pubmed.ncbi.nlm.nih.gov/32171076/)
6. Hellmuth J, Barnett TA, Asken BM, Kelly JD, Torres L, Stephens ML, et al. Persistent COVID-19-associated neurocognitive symptoms in non-hospitalized patients. *J Neurovirol*. 2021; 27: 191–195. <https://doi.org/10.1007/s13365-021-00954-4> PMID: [33528824](https://pubmed.ncbi.nlm.nih.gov/33528824/)
7. Graham EL, Clark JR, Orban ZS, Lim PH, Szymanski AL, Taylor C, et al. Persistent neurologic symptoms and cognitive dysfunction in non-hospitalized Covid-19 “long haulers.” *Ann Clin Transl Neurol*. 2021. <https://doi.org/10.1002/acn3.51350> PMID: [33755344](https://pubmed.ncbi.nlm.nih.gov/33755344/)
8. Lu R, Zhao X, Li J, Niu P, Yang B, Wu H, et al. Genomic characterisation and epidemiology of 2019 novel coronavirus: implications for virus origins and receptor binding. *The Lancet*. 2020; 395: 565–574. [https://doi.org/10.1016/S0140-6736\(20\)30251-8](https://doi.org/10.1016/S0140-6736(20)30251-8) PMID: [32007145](https://pubmed.ncbi.nlm.nih.gov/32007145/)
9. Zhou P, Yang X Lou, Wang XG, Hu B, Zhang L, Zhang W, et al. A pneumonia outbreak associated with a new coronavirus of probable bat origin. *Nature*. 2020; 579: 270–273. <https://doi.org/10.1038/s41586-020-2012-7> PMID: [32015507](https://pubmed.ncbi.nlm.nih.gov/32015507/)
10. Lakdawala SS, Menachery VD. The search for a COVID-19 animal model. *Science (1979)*. 2020; 368: 942–943. <https://doi.org/10.1126/science.abc6141>
11. Muñoz-Fontela C, Dowling WE, Funnell SGP, Gsell PS, Riveros-Balta AX, Albrecht RA, et al. Animal models for COVID-19. *Nature*. 2020; 586: 509–515. <https://doi.org/10.1038/s41586-020-2787-6> PMID: [32967005](https://pubmed.ncbi.nlm.nih.gov/32967005/)
12. McCray PB, Pewe L, Wohlford-Lenane C, Hickey M, Manzel L, Shi L, et al. Lethal Infection of K18-hACE2 Mice Infected with Severe Acute Respiratory Syndrome Coronavirus. *J Virol*. 2007. <https://doi.org/10.1128/jvi.02012-06> PMID: [17079315](https://pubmed.ncbi.nlm.nih.gov/17079315/)
13. Winkler ES, Bailey AL, Kafai NM, Nair S, McCune BT, Yu J, et al. SARS-CoV-2 infection of human ACE2-transgenic mice causes severe lung inflammation and impaired function. *Nat Immunol*. 2020; 21: 1327–1335. <https://doi.org/10.1038/s41590-020-0778-2> PMID: [32839612](https://pubmed.ncbi.nlm.nih.gov/32839612/)
14. Zheng J, Wong LYR, Li K, Verma AK, Ortiz ME, Wohlford-Lenane C, et al. COVID-19 treatments and pathogenesis including anosmia in K18-hACE2 mice. *Nature*. 2021; 589: 603–607. <https://doi.org/10.1038/s41586-020-2943-z> PMID: [33166988](https://pubmed.ncbi.nlm.nih.gov/33166988/)
15. Symptoms of COVID-19 | CDC. [cited 21 May 2021]. <https://www.cdc.gov/coronavirus/2019-ncov/symptoms-testing/symptoms.html>.
16. FDA Issues Emergency Use Authorization for Third COVID-19 Vaccine | FDA. [cited 26 Apr 2021]. <https://www.fda.gov/news-events/press-announcements/fda-issues-emergency-use-authorization-third-covid-19-vaccine>.
17. Coronavirus disease (COVID-19): Herd immunity, lockdowns and COVID-19. [cited 26 Apr 2021]. <https://www.who.int/news-room/q-a-detail/herd-immunity-lockdowns-and-covid-19>.
18. Rhoades A. Veklury (remdesivir) EUA Letter of Approval, reissued 10/22/2020. 2020.
19. Coronavirus (COVID-19) | Drugs | FDA. [cited 16 Jun 2023]. <https://www.fda.gov/drugs/emergency-preparedness-drugs/coronavirus-covid-19-drugs>.
20. Beigel JH, Tomashek KM, Dodd LE, Mehta AK, Zingman BS, Kalil AC, et al. Remdesivir for the Treatment of Covid-19—Final Report. *New England Journal of Medicine*. 2020; 383: 1813–1826. <https://doi.org/10.1056/NEJMoa2007764> PMID: [32445440](https://pubmed.ncbi.nlm.nih.gov/32445440/)
21. WHO recommends against the use of remdesivir in COVID-19 patients. [cited 25 Apr 2021]. <https://www.who.int/news-room/feature-stories/detail/who-recommends-against-the-use-of-remdesivir-in-covid-19-patients>.
22. Administration D. FDA Combating COVID-19 With Therapeutics. 2020.
23. Emergency Use Authorization | FDA. [cited 7 Mar 2023]. <https://www.fda.gov/emergency-preparedness-and-response/mcm-legal-regulatory-and-policy-framework/emergency-use-authorization#coviddrugs>.
24. Chirkov SN. The antiviral activity of chitosan (review). *Applied Biochemistry and Microbiology*. 2002. pp. 1–8. <https://doi.org/10.1023/A:1013206517442>

25. Mehrabi M, Montazeri H, Dounighi MN, Rashti A, Vakili-Ghartavol R. Chitosan-based nanoparticles in mucosal vaccine delivery. *Archives of Razi Institute. Razi Vaccine and Serum Research Institute*; 2018. pp. 165–176. <https://doi.org/10.22092/ari.2017.109235.1101>
26. Li X, Min M, Du N, Gu Y, Hode T, Naylor M, et al. Chitin, chitosan, and glycated chitosan regulate immune responses: The novel adjuvants for cancer vaccine. *Clinical and Developmental Immunology. Hindawi Limited*; 2013. <https://doi.org/10.1155/2013/387023> PMID: 23533454
27. Mudgal J, Mudgal PP, Kinra M, Raval R. Immunomodulatory role of chitosan-based nanoparticles and oligosaccharides in cyclophosphamide-treated mice. *Scand J Immunol.* 2019; 89: e12749. <https://doi.org/10.1111/sji.12749>
28. Carroll TD, Jegaskanda S, Matzinger SR, Fritts L, McChesney MB, Kent SJ, et al. A lipid/DNA adjuvant-inactivated influenza virus vaccine protects rhesus macaques from uncontrolled virus replication after heterosubtypic influenza a virus challenge. *Journal of Infectious Diseases.* 2018. <https://doi.org/10.1093/infdis/jiy238> PMID: 29701840
29. Lei X, Dong X, Ma R, Wang W, Xiao X, Tian Z, et al. Activation and evasion of type I interferon responses by SARS-CoV-2. *Nat Commun.* 2020; 11. <https://doi.org/10.1038/s41467-020-17665-9> PMID: 32733001
30. Xia H, Cao Z, Xie X, Zhang X, Chen JYC, Wang H, et al. Evasion of Type I Interferon by SARS-CoV-2. *Cell Rep.* 2020; 33. <https://doi.org/10.1016/j.celrep.2020.108234> PMID: 32979938
31. S Ribero M, Jouvenet N, Dreux M, Nisole S. Interplay between SARS-CoV-2 and the type I interferon response. *PLoS Pathogens. Public Library of Science*; 2020. <https://doi.org/10.1371/journal.ppat.1008737> PMID: 32726355
32. Zheng M, Qu D, Wang H, Sun Z, Liu X, Chen J, et al. Intranasal Administration of Chitosan Against Influenza A (H7N9) Virus Infection in a Mouse Model. *Sci Rep.* 2016; 6. <https://doi.org/10.1038/srep28729> PMID: 27353250
33. Wang X, Zhang W, Liu F, Zheng M, Zheng D, Zhang T, et al. Intranasal immunization with live attenuated influenza vaccine plus chitosan as an adjuvant protects mice against homologous and heterologous virus challenge. *Arch Virol.* 2012; 157: 1451–1461. <https://doi.org/10.1007/s00705-012-1318-7>
34. Choi B, Jo DH, Anower AKMM, Islam SMS, Sohn S. Chitosan as an Immunomodulating Adjuvant on T-Cells and Antigen-Presenting Cells in Herpes Simplex Virus Type 1 Infection. *Mediators Inflamm.* 2016; 2016. <https://doi.org/10.1155/2016/4374375> PMID: 28096567
35. Kim SJ, Nguyen VG, Kim CU, Park BK, Le Huynh TM, Shin S, et al. Application of chitosan as a natural disinfectant against porcine epidemic diarrhoea virus. *Acta Vet Hung.* 2021; 69: 94–99. <https://doi.org/10.1556/004.2021.00001>
36. Pyrc K, Milewska A, Duran EB, Botwina P, Dabrowska A, Jedrysiak M, et al. SARS-CoV-2 inhibition using a mucoadhesive, amphiphilic chitosan that may serve as an anti-viral nasal spray. *Sci Rep.* 2021; 11. <https://doi.org/10.1038/s41598-021-99404-8> PMID: 34625610
37. Jaber N, Al-Remawi M, Al-Akayleh F, Al-Muhtaseb N, Al-Adham ISI, Collier PJ. A review of the antiviral activity of Chitosan, including patented applications and its potential use against COVID-19. *J Appl Microbiol.* 2022; 132: 41–58. <https://doi.org/10.1111/jam.15202> PMID: 34218488
38. Safarzadeh M, Sadeghi S, Azizi M, Rastegari-Pouyani M, Pouriran R, Haji Molla Hoseini M. Chitin and chitosan as tools to combat COVID-19: A triple approach. *Int J Biol Macromol.* 2021; 183: 235–244. <https://doi.org/10.1016/j.ijbiomac.2021.04.157> PMID: 33930442
39. Sharma N, Modak C, Singh PK, Kumar R, Khatri D, Singh SB. Underscoring the immense potential of chitosan in fighting a wide spectrum of viruses: A plausible molecule against SARS-CoV-2? *Int J Biol Macromol.* 2021; 179: 33–44. <https://doi.org/10.1016/j.ijbiomac.2021.02.090> PMID: 33607132
40. Zhuo S-H, Wu J-J, Zhao L, Li W-H, Zhao Y-F, Li Y-M. A chitosan-mediated inhalable nanovaccine against SARS-CoV-2. *Nano Res.* 2022; 15: 4191–4200. <https://doi.org/10.1007/s12274-021-4012-9> PMID: 35126879
41. Tan RSL, Hassandarvish P, Chee CF, Chan LW, Wong TW. Chitosan and its derivatives as polymeric anti-viral therapeutics and potential anti-SARS-CoV-2 nanomedicine. *Carbohydr Polym.* 2022; 290: 119500. <https://doi.org/10.1016/j.carbpol.2022.119500> PMID: 35550778
42. Chen WR, Carubelli R, Liu H, Nordquist RE. Laser immunotherapy: A novel treatment modality for metastatic tumors. *Applied Biochemistry and Biotechnology—Part B Molecular Biotechnology.* 2003; 25: 37–43. <https://doi.org/10.1385/MB:25:1:37>
43. Song S, Zhou F, Nordquist RE, Carubelli R, Liu H, Chen WR. Glycated chitosan as a new non-toxic immunological stimulant Glycated chitosan immunological stimulant. *Immunopharmacol Immunotoxicol.* 2009; 31: 202–208. <https://doi.org/10.1080/08923970802629593> PMID: 19514994

44. Zizzari I, Napoletano C, Battisti F, Rahimi H, Caponnetto S, Pierelli L, et al. MGL Receptor and Immunity: When the Ligand Can Make the Difference. *J Immunol Res*. 2015;2015. <https://doi.org/10.1155/2015/450695> PMID: 26839900
45. Korbelik M, Banáth J, Zhang W, Hode T, Lam S, Gallagher P, et al. N-dihydrogalactochitosan-supported tumor control by photothermal therapy and photothermal therapy-generated vaccine. *J Photochem Photobiol B*. 2020; 204. <https://doi.org/10.1016/J.JPHOTOBIOB.2020.111780>
46. Korbelik M, Hode T, Lam SSK, Chen WR. Novel Immune Stimulant Amplifies Direct Tumoricidal Effect of Cancer Ablation Therapies and Their Systemic Antitumor Immune Efficacy. *Cells*. NLM (Medline); 2021. <https://doi.org/10.3390/cells10030492> PMID: 33668932
47. Qi S, Lu L, Zhou F, Chen Y, Xu M, Chen L, et al. Neutrophil infiltration and whole-cell vaccine elicited by N-dihydrogalactochitosan combined with NIR phototherapy to enhance antitumor immune response and T cell immune memory. *Theranostics*. 2020; 10: 1814–1832. <https://doi.org/10.7150/thno.38515> PMID: 32042338
48. Zhou F, Yang J, Zhang Y, Liu M, Lang ML, Li M, et al. Local phototherapy synergizes with immunoadjuvant for treatment of pancreatic cancer through induced immunogenic tumor vaccine. *Clinical Cancer Research*. 2018; 24: 5335–5346. <https://doi.org/10.1158/1078-0432.CCR-18-1126> PMID: 30068705
49. El-Hussein A, Lam SSK, Raker J, Chen WR, Hamblin MR. N-dihydrogalactochitosan as a potent immune activator for dendritic cells. *J Biomed Mater Res A*. 2017; 105: 963–972. <https://doi.org/10.1002/jbm.a.35991> PMID: 28028922
50. Hoover AR, Liu K, Devette CI, Krawic JR, West CL, Medcalf D, et al. ScRNA-seq reveals tumor microenvironment remodeling induced by local intervention-based immunotherapy. *bioRxiv*. 2020; 2020.10.02.323006. <https://doi.org/10.1101/2020.10.02.323006>
51. Hoover AR, More S, Liu K, West CL, Valero TI, Yu N, et al. A novel biopolymer for mucosal adjuvant against respiratory pathogens. *bioRxiv*. 2022; 2022.09.07.506979. <https://doi.org/10.1101/2022.09.07.506979>
52. Brown C, Vostok J, Johnson H, Burns M, Gharpure R, Sami S, et al. Outbreak of SARS-CoV-2 Infections, Including COVID-19 Vaccine Breakthrough Infections, Associated with Large Public Gatherings—Barnstable County, Massachusetts, July 2021. *MMWR Morb Mortal Wkly Rep*. 2021; 70: 1059–1062. <https://doi.org/10.15585/mmwr.mm7031e2> PMID: 34351882
53. Bellich B, D'Agostino I, Semeraro S, Gamini A, Cesàro A. “The Good, the Bad and the Ugly” of Chitosans. *Mar Drugs*. 2016; 14. <https://doi.org/10.3390/md14050099> PMID: 27196916
54. Jayathilakan K, Sultana K, Radhakrishna K, Bawa AS. Utilization of byproducts and waste materials from meat, poultry and fish processing industries: A review. *Journal of Food Science and Technology*. *J Food Sci Technol*; 2012. pp. 278–293. <https://doi.org/10.1007/s13197-011-0290-7> PMID: 23729848
55. Negm NA, Hefni HHH, Abd-Elalal AAA, Badr EA, Abou Kana MTH. Advancement on modification of chitosan biopolymer and its potential applications. *International Journal of Biological Macromolecules*. Elsevier B.V.; 2020. pp. 681–702. <https://doi.org/10.1016/j.ijbiomac.2020.02.196> PMID: 32084486
56. Mokhtar H, Biffar L, Somavarapu S, Frossard JP, McGowan S, Pedrera M, et al. Evaluation of hydrophobic chitosan-based particulate formulations of porcine reproductive and respiratory syndrome virus vaccine candidate T cell antigens. *Vet Microbiol*. 2017; 209: 66–74. <https://doi.org/10.1016/j.vetmic.2017.01.037> PMID: 28228336
57. Shim S, Park HE, Soh SH, Im Y Bin, Yoo HS. Induction of Th2 response through TLR2-mediated MyD88-dependent pathway in human microfold cells stimulated with chitosan nanoparticles loaded with *Brucella abortus* Mdh. *Microb Pathog*. 2020; 142. <https://doi.org/10.1016/j.micpath.2020.104040> PMID: 32032767
58. Zhang X, Wu K, Wang D, Yue X, Song D, Zhu Y, et al. Nucleocapsid protein of SARS-CoV activates interleukin-6 expression through cellular transcription factor NF- $\kappa$ B. *Virology*. 2007; 365: 324–335. <https://doi.org/10.1016/j.virol.2007.04.009> PMID: 17490702
59. Blanco-Melo D, Nilsson-Payant BE, Liu WC, Uhl S, Hoagland D, Møller R, et al. Imbalanced Host Response to SARS-CoV-2 Drives Development of COVID-19. *Cell*. 2020; 181: 1036–1045.e9. <https://doi.org/10.1016/j.cell.2020.04.026> PMID: 32416070
60. Pyle C, Uwadiae F, Swieboda D, Harker J. Early IL-6 signalling promotes IL-27 dependent maturation of regulatory T cells in the lungs and resolution of viral immunopathology. *PLoS Pathog*. 2017; 13. <https://doi.org/10.1371/journal.ppat.1006640> PMID: 28953978
61. Bueter CL, Lee CK, Rathinam VAK, Healy GJ, Taron CH, Specht CA, et al. Chitosan but not chitin activates the inflammasome by a mechanism dependent upon phagocytosis. *Journal of Biological Chemistry*. 2011; 286: 35447–35455. <https://doi.org/10.1074/jbc.M111.274936> PMID: 21862582
62. Carroll EC, Jin L, Mori A, Muñoz-Wolf N, Oleszycka E, Moran HBT, et al. The Vaccine Adjuvant Chitosan Promotes Cellular Immunity via DNA Sensor cGAS-STING-Dependent Induction of Type I Interferons. *Immunity*. 2016; 44: 597–608. <https://doi.org/10.1016/j.immuni.2016.02.004> PMID: 26944200

63. Sun B, Yu S, Zhao D, Guo S, Wang X, Zhao K. Polysaccharides as vaccine adjuvants. *Vaccine*. Elsevier Ltd; 2018. pp. 5226–5234. <https://doi.org/10.1016/j.vaccine.2018.07.040> PMID: 30057282
64. Read RC, Naylor SC, Potter CW, Bond J, Jabbal-Gill I, Fisher A, et al. Effective nasal influenza vaccine delivery using chitosan. *Vaccine*. 2005; 23: 4367–4374. <https://doi.org/10.1016/j.vaccine.2005.04.021> PMID: 15916838
65. Elieh Ali Komi D, Sharma L, Dela Cruz CS. Chitin and Its Effects on Inflammatory and Immune Responses. *Clinical Reviews in Allergy and Immunology*. Humana Press Inc.; 2018. pp. 213–223. <https://doi.org/10.1007/s12016-017-8600-0> PMID: 28251581
66. Bashiri S, Koirala P, Toth I, Skwarczynski M. Carbohydrate immune adjuvants in subunit vaccines. *Pharmaceutics*. MDPI AG; 2020. pp. 1–33. <https://doi.org/10.3390/pharmaceutics12100965> PMID: 33066594
67. Bueter CL, Specht CA, Levitz SM. Innate Sensing of Chitin and Chitosan. *PLoS Pathog*. 2013; 9. <https://doi.org/10.1371/journal.ppat.1003080> PMID: 23326227
68. Seetharaman J, Kfanigsberg A, Slaaby R, Leffler H, Barondes SH, Rini JM. X-ray crystal structure of the human galectin-3 carbohydrate recognition domain at 2.1-Å resolution. *Journal of Biological Chemistry*. 1998; 273: 13047–13052. <https://doi.org/10.1074/jbc.273.21.13047> PMID: 9582341
69. Semeňuk T, Krist P, Pavlíček J, Bezouška K, Kuzma M, Novák P, et al. Synthesis of chito oligomer-based glycoconjugates and their binding to the rat natural killer cell activation receptor NKR-P1. *Glycoconj J*. 2001; 18: 817–826. <https://doi.org/10.1023/a:1021111703443> PMID: 12441671
70. Zhou F, Wu S, Song S, Chen WR, Resasco DE, Xing D. Antitumor immunologically modified carbon nanotubes for photothermal therapy. *Biomaterials*. 2012; 33: 3235–3242. <https://doi.org/10.1016/j.biomaterials.2011.12.029> PMID: 22296829
71. Nevagi RJ, Khalil ZG, Hussein WM, Powell J, Batzloff MR, Capon RJ, et al. Polyglutamic acid-trimethyl chitosan-based intranasal peptide nano-vaccine induces potent immune responses against group A streptococcus. *Acta Biomater*. 2018; 80: 278–287. <https://doi.org/10.1016/j.actbio.2018.09.037> PMID: 30266637
72. Micoli F, Costantino P, Adamo R. Potential targets for next generation antimicrobial glycoconjugate vaccines. *FEMS Microbiology Reviews*. Oxford University Press; 2018. pp. 388–423. <https://doi.org/10.1093/femsre/fuy011> PMID: 29547971
73. Korbelik M, Hode T, Lam SSK, Chen WR. Novel Immune Stimulant Amplifies Direct Tumoricidal Effect of Cancer Ablation Therapies and Their Systemic Antitumor Immune Efficacy. *Cells*. 2021; 10: 1–9. <https://doi.org/10.3390/cells10030492> PMID: 33668932
74. Li X, Naylor MF, Le H, Nordquist RE, Teague TK, Howard CA, et al. Clinical effects of in situ photoimmunotherapy on late-stage melanoma patients: a preliminary study. *Cancer Biol Ther*. 2010; 10: 1081–1087. <https://doi.org/10.4161/cbt.10.11.13434> PMID: 20890121
75. Li X, Ferrel GL, Guerra MC, Hode T, Lunn JA, Adalsteinsson O, et al. Preliminary safety and efficacy results of laser immunotherapy for the treatment of metastatic breast cancer patients. *Photochem Photobiol Sci*. 2011; 10: 817. <https://doi.org/10.1039/c0pp00306a> PMID: 21373701
76. Meng Q, Sun Y, Cong H, Hu H, Xu FJ. An overview of chitosan and its application in infectious diseases. *Drug Deliv Transl Res*. 2021; 11: 1340–1351. <https://doi.org/10.1007/s13346-021-00913-w> PMID: 33496926
77. Bello-Morales R, Andreu S, Ruiz-Carpio V, Ripa I, López-Guerrero JA. Extracellular Polymeric Substances: Still Promising Antivirals. *Viruses*. 2022; 14. <https://doi.org/10.3390/v14061337> PMID: 35746808
78. Gopal J, Muthu M, Pushparaj SSC, Sivanesan I. Anti-COVID-19 Credentials of Chitosan Composites and Derivatives: Future Scope? *Antibiotics (Basel)*. 2023; 12. <https://doi.org/10.3390/antibiotics12040665> PMID: 37107027
79. National Institutes of Health. GUIDE LABORATORY ANIMALS FOR THE CARE AND USE OF Eighth Edition Committee for the Update of the Guide for the Care and Use of Laboratory Animals Institute for Laboratory Animal Research Division on Earth and Life Studies. 2011 [cited 6 Mar 2023]. <http://www.nap.edu>.
80. Cisney ED, Fernandez S, Hall SI, Krietz GA, Ulrich RG. Examining the role of nasopharyngeal-associated lymphoreticular tissue (NALT) in mouse responses to vaccines. *J Vis Exp*. 2012 [cited 6 Mar 2023]. <https://doi.org/10.3791/3960> PMID: 22871688